Journal of
Marine Science and Engineering

MDPI

Article

Design and Analysis of a Sub-Surface Longline Marine Aquaculture Farm for Co-Existence with Offshore Wind Farm

Sung Youn Boo [1,*], Steffen Allan Shelley [1], Seung-Ho Shin [2], Jiyong Park [2] and Yoon-Jin Ha [2]

[1] VL Offshore LLC, Houston, TX 77084, USA; sshelley@vloffshore.com
[2] Korea Research Institute of Ships & Ocean Engineering (KRISO), Daejeon 34103, Republic of Korea; shinsh@kriso.re.kr (S.-H.S.); jypark@kriso.re.kr (J.P.); yj_ha0811@kriso.re.kr (Y.-J.H.)
* Correspondence: sboo@vloffshore.com

Abstract: There has been growing interest recently in hybrid installations integrating the offshore wind farm and aquaculture farm as co-existence while optimizing ocean space use. The offshore marine farms beyond coastal or sheltered areas will require mooring to ensure the station-keeping of the farm system during the storms. In the present work, a sub-surface longline farm is installed in a fixed offshore wind farm at a distance from the wind foundations. The farm is designed to cultivate oysters in multi-compartment bags attached to the longlines vertically. The farm with a cultivating area of 200 m × 200 m is supported by the various farm lines made of polypropylene and buoys that is moored with catenary mooring arrangements. Drag coefficients of a full-scale oyster bag in wave and current are determined using the results of wave basin tests. A lumped model is developed and validated with a complete model for a partial farm. The lumped model is used to simulate the coupled responses of the whole farm in the site extreme waves and currents of a 50-year return period. The strength and fatigue designs of the mooring and farm lines are evaluated against the industry standards and confirmed to comply with the design requirements.

Keywords: marine culture farm; offshore aquaculture; lumped model; mooring; longline; co-existence

Citation: Boo, S.Y.; Shelley, S.A.; Shin, S.-H.; Park, J.; Ha, Y.-J. Design and Analysis of a Sub-Surface Longline Marine Aquaculture Farm for Co-Existence with Offshore Wind Farm. *J. Mar. Sci. Eng.* **2023**, *11*, 1034. https://doi.org/10.3390/jmse11051034

Academic Editor: Nitai Drimer

Received: 9 April 2023
Revised: 1 May 2023
Accepted: 9 May 2023
Published: 12 May 2023

1. Introduction

Installations of offshore wind farms may be inevitable but they have faced social challenges from the fishery industries and other stakeholders [1,2]. The co-existence of an integrated (or hybrid) farm by combining the wind and marine aquaculture may be an alternative to ease the social and economic challenges. Therefore, an integrated farm concept implementing offshore wind energy and marine cultivation has drawn interest among policy makers, scientists, the aquaculture industry, and other stakeholders, and it has been studied throughout the world in places such as Europe, the USA, and Asia [3].

Many different concepts of the integrated farm have been proposed [4]. A marine aquaculture concept for co-existence can be differentiated with mainly three concepts, depending on the marine farm mooring configurations: installation of the marine farm using an independent mooring system at a safe distance from the turbine foundation boundary [5]; a direct mooring connection to the neighboring wind foundation structure [6]; and a direct integration of the cage farm to the turbine foundation [7,8]. The first method co-locates the marine culture farm near existing wind structures, but does not directly connect to the wind farm structures and offers a safe zone from the wind turbine structure with corridors for support vessels to access the marine culture farm or the wind farm. However, the system requires its own mooring lines and anchors with their associated additional costs. The second and third concepts utilize the wind turbine foundation as a mooring anchor for the marine farm by connecting the longlines directly to the turbine structures. In some cases, a small individual cultivating unit is tied to the foundation or placed inside the floating platform with multiple column structures [5]. There is a significant cost benefit

to removing the marine culture farm anchor system, but dynamic loads from the marine culture system are transferred to the wind turbine structures, which can affect the wind foundation structural strength or fatigue around the connection points. For floating wind installations, the floating platform dynamics are affected by the aquaculture line, resulting in complex load coupling between the longlines and the turbine platform. This impact may need to be considered in the wind turbine foundation design phase rather than the post-analysis after the turbine platform installation.

The use of a longline scheme is a well-implemented marine culture practice for a large floating marine farm [4], although there are many design factors to be considered for an open water site [9]. Various numerical methods have been developed to analyze the coupling of the longline, culturing units, buoys, and anchor lines by means of a lumped model under waves and currents [10], or else a mass-based model for kelp longline [11]. A single longline is typically used to develop a numerical method or analyze the coupling [12–14]. Among them, an open-source code MoorDyn is further modified for a single mussel line [12]. Hydro-FE is also applied to the single longline for a mussel installation. In both cases, the longline used is about 100 m long, which is shorter than a typical full-scale length. There are approaches to consider current effects to the longline farm system [15] or mooring tensions [11] that address the longline tension that is observed to be sensitive to the tide water level.

The numerical model requires the drag and inertia coefficients of the culturing species as input to run the coupled analysis under wave and current. The coefficients vary depending on the species, size, and many other factors. Laboratory measurements in waves or currents are conducted for oyster trays stacked vertically [16], mussel dropper lines [17,18], longline and mooring tension [19], and drag load on the line [20]. Due to a limitation of test facilities, the majority of the laboratory tests are conducted with wave or current rather than combined environments of wave and current together. A full-scale field test is another option, as it may be a more reliable method to estimate the load on the line or to verify the engineering design than the test with a scaled model. Feasibility of the longline is investigated with a field test [21], where some issues of two different line materials of polypropylene and steel wire are discussed. Motions and loading on a submerged mussel longline are measured at an open sea site [22]. There is also research on the net cage for fish, and the analysis and measurements for the cage farm are relevant to the ocean engineering field in order to estimate the cage responses and the mooring behaviors for multiple cages [23–26] or single cages [27,28].

An offshore aquaculture farm in Korea will, according to plans, be installed in a fixed offshore wind farm to demonstrate the co-existence, as depicted in Figure 1. The sub-surface longline marine farm is 10 km off the south-west shore of Korea. Before the commercial scale farm installation, a pilot size farm with 200 m $\times$ 200 m will be considered. This size farm has been widely used in Korea in coastal and sheltered areas. However, the offshore farm is situated in the open ocean, having much harsher environments than the sheltered farms.

The marine farm will be used to cultivate various species of shellfish, kelps, or seaweed. For the present analysis, an oyster farm is considered. The farm is a floating system consisting of various lines, buoys, anchors, and oyster bags, and it is moored with anchor lines and drag anchors. It is considered that no lines consisting of the marine farm are connected to the wind turbine structures. There is a sufficient safe zone between the marine farm and the wind farm to prevent potential interferences during the storm.

Drag coefficients of the oyster bag with marine growth are determined from a full-scale wave basin test for fixed and free-hanging bags under the wave and current, independently. The drag coefficient for a wave and current combined case is then estimated. The coefficients are used for the numerical model constructed by OrcaFlex [29].

Therefore, to reduce the numerical overburden in the time domain, a lumped method, by lumping the oyster bags and the longline buoys, is implemented. The lumped model is validated with a complete partial farm, and it is then extended to model the whole farm

in order to calculate the loads on the farm lines and the anchor lines. The site has very strong current with a high tidal level variation. Typhoons occasionally pass through the site during the summer and fall seasons. Thus, the Design Load Cases (DLCs) are constructed accordingly to consider the wave dominant and current dominant cases [30] separately, along with the tide level variations. The water depth of the site is about 11.8 m. The typical submergence of the longline is about 5 to 10 m to reduce the wave effect to the culturing species, but, for the present analysis, a submergence of 1.5 m is considered, based on the factors of the shallow depth with a high variation of tide and typhoon wave heights, in order to avoid a potential clash of the oyster bags with the seafloor.

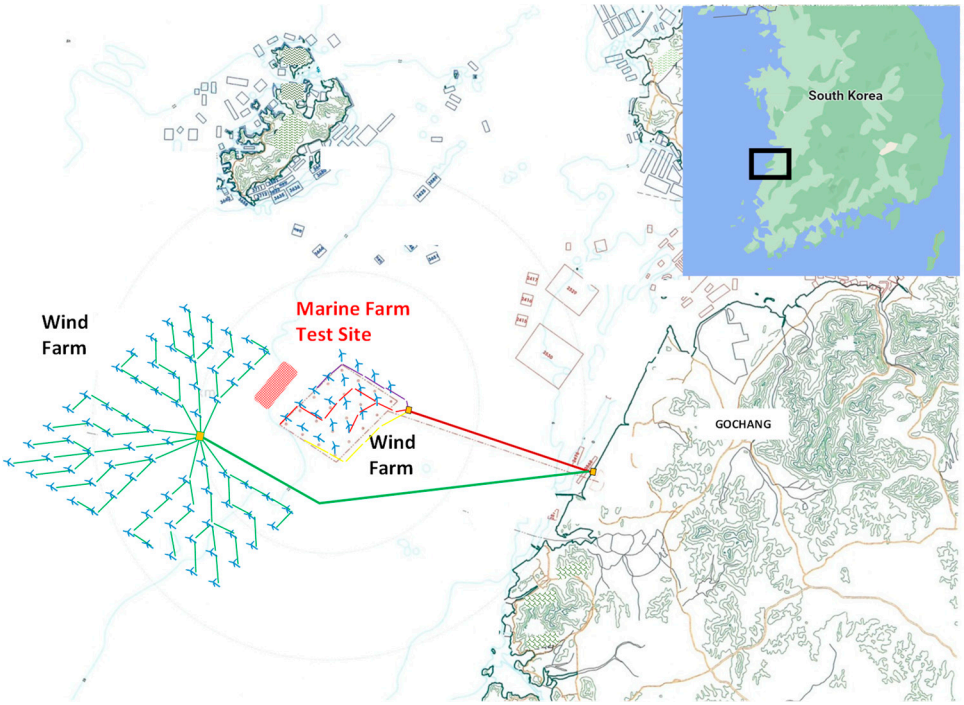

Figure 1. Marine aquaculture farm site located off the SW Korean offshore inside a fixed wind farm.

Objectives of the present work are: (1) to determine the drag coefficients of the oyster bag using the wave basin test with a full-scale oyster bag; (2) to develop a numerical scheme of a lumped model effectively in order to conduct the longline farm analysis; (3) to conduct the numerical simulation of the offshore pilot farm under 50-year extreme environments; and (4) to confirm the strength and fatigue design of the farm lines against the design standards.

The standards recommended include DNV [31–33], ABS [34], ISO [35], and Norwegian standard [30]. Among them, the DNV standard and recommendation [31–33] are chosen and used for the design check. The farm is designed to comply with the requirements in the Ultimate Limit State (ULS) and the Fatigue Limit State (FLS) of DNV.

2. Basis of Design Summary

2.1. Extreme Conditions and Design Load Cases

The designed extreme condition of ULS considers a 50-yr sea [36]. According to NS9415 [30], the 50-yr waves and 10-yr currents can be combined for a wave dominant and current dominant conditions in the ULS. The resulting extreme wave with JONSAWP parameters and currents are summarized in Table 1. Co-directional environments are considered for the ULS according to NS9415 [30], while misaligned directions are used for the FLS based on the directionalities of the site dominant waves and currents. Winds are excluded as the farm system, except for the buoys, is submerged. The site water depth

varies due to the water levels of the Mean Sea Level (MSL), Highest Still Water Level (HSWL), and Lowest Still Water Level (LSWL), which are included in Table 1.

Table 1. Combined waves and currents for ULS.

Parameters	Wave Dominant	Current Dominant
Significant wave height, Hs (m)	5.97	4.18
Max wave height, Hmax (m)	11.10	7.77
Peak period, Tp (m/s)	11.16	11.16
Gamma	1.64	1.64
Current @ surface (m/s)	0.98	1.10
Water Level, MSL/HSWL/LSWL (m)	11.8/16.2/8.3	11.8/16.2/8.3

Regular (design) waves are derived from the irregular waves in Table 1. The site water depth becomes shallow, especially during a low tide, which may cause wave breaking. When the breaking wave occurs, the regular wave height is recalculated not to exceed the breaking wave limit. The resulting regular waves for the 50-yr extreme are summarized in Table 2 and they are used for the present analysis. Table 3 summarizes the design load cases that are a combination of regular wave height H and period T, currents, and water levels for the wave dominant and current dominant cases.

Table 2. Regular waves for various water levels (ULS).

Parameters	LSWL	MSL	HSWL
Water level (depth) (m)	8.3	11.8	16.2
Wave height: wave dominant (m)	6.04	8.31	10.93
: current dominant (m)	6.04	7.77	7.77
Period (s)	11.16	11.16	11.16

Table 3. Design load cases with regular waves and current combinations (ULS).

DLC	H (m)	T (m/s)	Current (m/s)	Water Depth (m)	Note
DLC-WL	6.04	11.16	0.98	8.3	Wave dom., LSWL
DLC-WM	8.31	11.16	0.98	11.8	Wave dom., MSL
DLC-WH	10.93	11.16	0.98	16.2	Wave dom., HSWL
DLC-CL	6.04	11.16	1.10	8.3	Current dom., LSWL
DLC-CM	7.77	11.16	1.10	11.8	Current dom., MSL
DLC-CH	7.77	11.16	1.10	16.2	Current dom., HSWL

2.2. Farm Line Design Criteria

The mooring lines and other marine farm lines will be designed to comply with the requirements specified by DNV [32], such that the Utilization Factor (UF) shall not exceed 1.0, as provided in Equation (2):

$$UF = \left(T_{mean} \times \gamma_{mean} + T_{dyn} \times \gamma_{dyn}\right) / S_c \quad (1)$$

$$UF < 1.0 \quad (2)$$

where S_c is characteristic strength, T_{mean} is characteristic mean line tension due to pretension and mean environmental actions, T_{dyn} is characteristic dynamic line tension, γ_{mean} is partial safety factor on mean tension, and γ_{dyn} is partial safety factor on dynamic tension. The partial safety factors for ULS are γ_{mean} = 1.1 and γ_{dyn} = 1.5. The present farm mooring system is considered as Consequence Class 1 [32]. The fatigue life of the farm lines shall meet the requirement with a safety factor of 60.

3. Marine Aquaculture Farm Configuration and Modeling Set-Up

3.1. Farm Configuration

An offshore marine culture farm with dimensions of 200 m × 200 m is constructed with synthetic polypropylene ropes. The farm system consists of the farm lines (mooring anchor lines, main lines, longlines, crosslines, and buoy lines), mooring anchors, oyster bags, and buoys. Anchor lines are connected to the main lines. Some anchor lines are in groups of three so that they can share the concentrated loads. The main lines are supported by the main buoys and the side support buoys, while the longlines and oyster bags are supported by the longline buoys. The oyster bags are tied to the longline at 1 m spacing between the bags. Therefore, a total of 199 oyster bags are installed on each longline. An individual drag anchor is used for each anchor line. Due to the almost neutral buoyant anchor lines, a clump weight of 8 kg is attached at 20 m from the top end of each anchor line. Tables 4–6 present the properties of the farm line components.

Table 4. Marine culture farm line (polypropylene rope) properties.

Components	Length m	OD mm	Weight kg/m	MBL kN	Spacing m
Main line, each	200	48	0.93	306.2	200
Longline, each	200	36	0.52	175.6	20
Cross line, each	200	48	0.93	306.2	28~30
Anchor line, each	61	36	0.52	175.6	Varies
Main buoy line, each	1.5	16	0.13	29.8	50~60
Side support buoy line, each	1.5	12	0.07	17.4	10
Longline buoy line, each	1.5	9	0.04	10.2	2
Oyster bag line, each	0.1	9	0.04	10.2	1
Oyster bag line used for model test	1.0	8	0.03	8.3	N/a

Table 5. Marine aquaculture farm buoy properties.

Buoy Name	Volume m^3	Weight in Air kg	Spacing m
Main buoy (corner)	0.42	9.04	50~60
Side support buoy	0.20	8.46	10
Longline buoy	0.06	2.92	2

Table 6. Oyster bag properties.

Oyster Bag	Length m	OD cm	Weight in Air kg	Weight in Water kg	Spacing m	Total of Bags
Non-marine growth	1.25	40	33.8	10.33	1	199
Marine growth	1.25	48	50.0	18.43	1	199

3.2. Marine Aquaculture Farm Notations

The marine farm is oriented toward the current direction such that the longline direction is normal to the tidal current direction (Figure 2), which may minimize potential clashing between the oyster bags due to the waves and currents. The wave and current heading ("flowing to") is defined from the farm east in counterclockwise. The positive x-axis is aligned to the longline direction, and the reference center of the z-coordinate is located at the MSL.

To identify the farm lines, the main lines, longlines, crosslines, and anchor lines are notated and numbered in Figure 2. The anchor lines are configured with a straight line and angled lines. The angled anchor lines in the grouped lines are tied to the straight-line end on the main lines. For example, N1, N1W, and N1E are tied to the same location on the main line. Here, N1W and N1E indicate the west and east (angled) side lines to the N1 (straight) line. The angled line notations are omitted for clarity. Other line notations are omitted for reasons of self-explanation. The crosslines are tightly connected to the longlines at the

crossing points. As shown, a high number of the anchor lines are distributed alongside the farm boundary. This can contribute to reducing the anchor line tensions, resulting in an anchor load level such that, first, a small size anchor readily available domestically in Korea can be utilized and, second, the anchor failure effect to the farm during a typhoon or storm may be minimized.

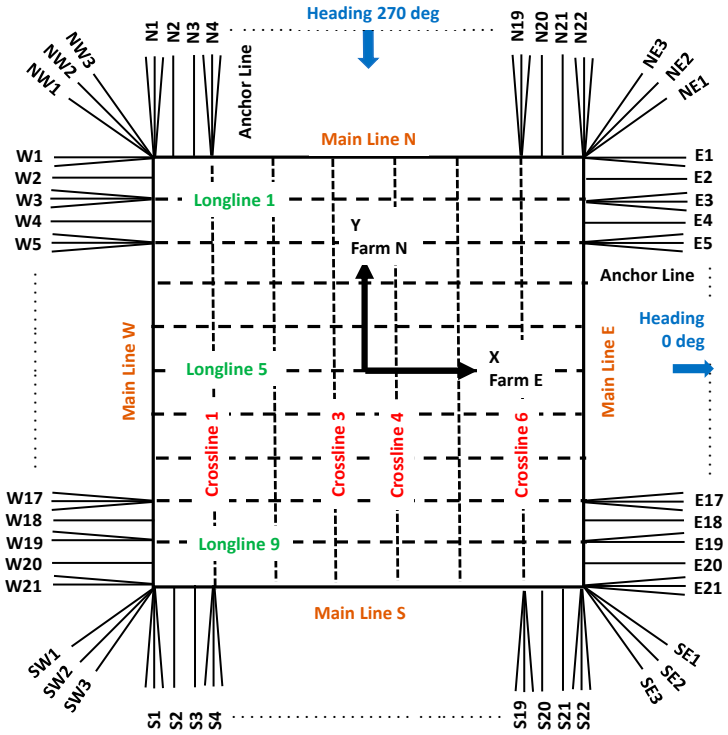

Figure 2. Notation and numbering of main line, longline, crossline, and anchor line. Environmental heading and reference coordinates are defined.

A part of the farm is shown in Figures 3 and 4, where the main buoys, side support buoys, longline buoys, oyster bags, associated line lengths, and spacings are presented. Main buoys (green) are distributed 50 to 60 m apart on the main lines while the side support buoys (red) are distributed every 10 m spacing. The longline buoys (yellow) are distributed every 2 m along the longlines. The spacing between the 1.25 m long oyster bags is 1 m. The marine farm is designed to be submerged at 1.5 m so that length of each buoy line used is 1.5 m.

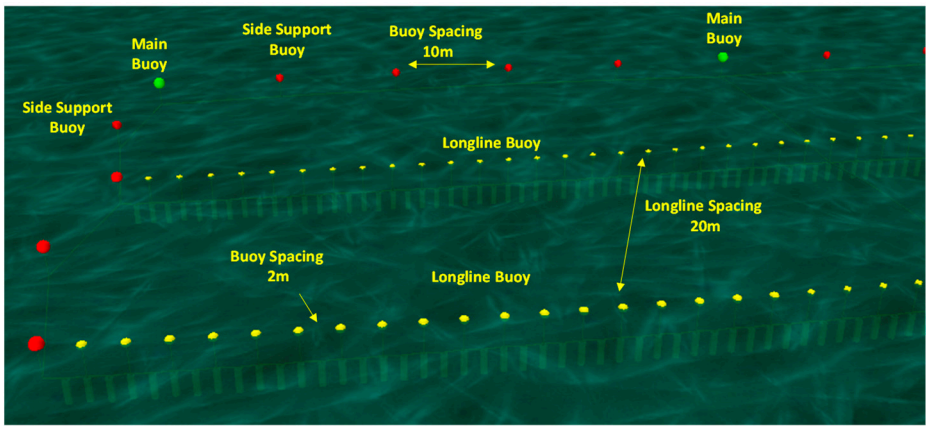

Figure 3. Main buoys (green) and side support buoys (red) distributed on the main lines. Longline (yellow) buoys distributed on the longlines.

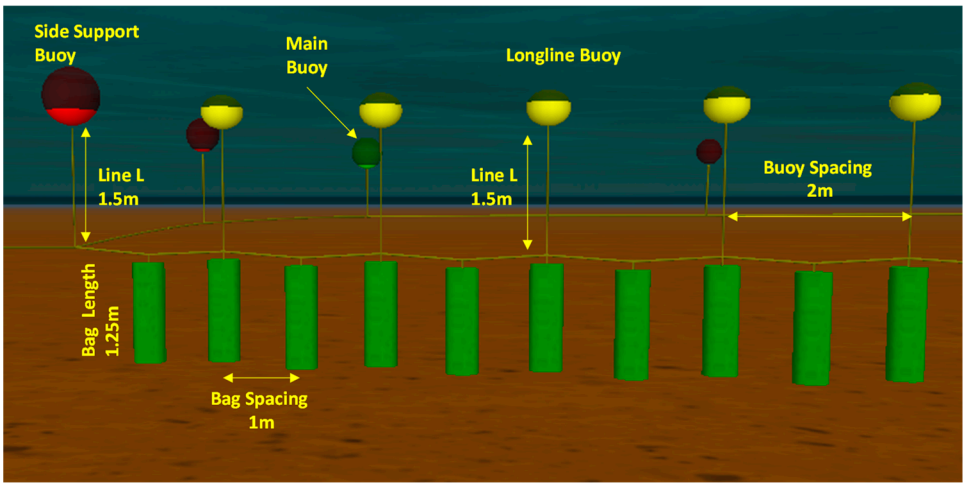

Figure 4. Main buoys (green), side support buoys (red), oyster bag (green), and associated line lengths and spacings.

4. Wave Basin Test and Drag Coefficient Correlation

4.1. Wave Basin Test Set-Up

The series of tests was conducted at the Ocean Wave Basin in KRISO [37], using a full-scale single oyster bag to determine the drag coefficients of the bag. The tests under various current and wave conditions were repeated for both non-marine growth and marine growth bags in Figure 5a,b. However, the marine growth results were selected for the present numerical analysis. Two different oyster bag configurations were considered: a fixed bag and a free hanging bag. The properties of the bag line used for the model test are provided in Table 4. The line ends of the submerged fixed bag were fixed while the bottom end of the free-hanging bag was set free. The bag was towed at various current (tow) speeds and the forces were measured. The tow tests that were captured are presented in Figure 5c,d. Line tensions and the angle of inclination of the bag were measured for the free hanging bag tests. Tensions on the free hanging bag were also measured for the regular waves without towing.

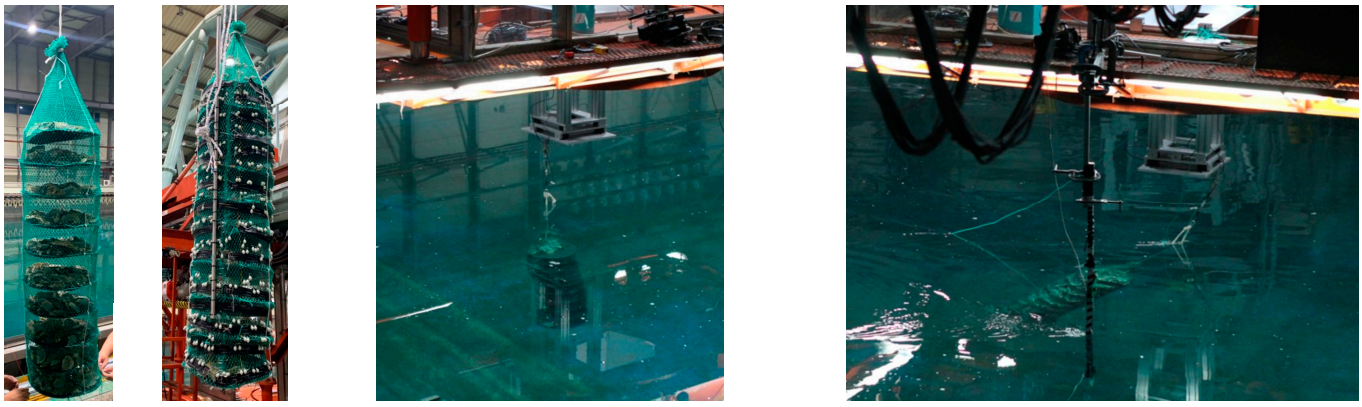

(**a**) (**b**) (**c**) (**d**)

Figure 5. Wave basin test: (**a**) non-marine growth bag; (**b**) marine growth bag; (**c**) fixed oyster bag case tow test; (**d**) free-hanging oyster bag tow test.

In the numerical correlation using the measured data, the same current speeds and waves used for the wave basin model tests were applied, and then the normal drag and axial (tangential) drag coefficients of the oyster bags were iteratively determined until the numerical forces converge with the measured values.

4.2. Drag Coefficients under Current

The measured and simulated tensions are compared in Figure 6, where the simulated values are based on the correlated coefficients in normal and axial (tangential) directions. Differences between measurements and numerical results are within 1%, except the free-hanging case for a current 0.5 m/s, which presents about 20%. The normal drag coefficient is estimated to be 1.0 for the tested currents, whereas the axial drags coefficients decrease quickly as the current speed becomes higher. The measured normal drag coefficients of 1.0 is close to a value of 1.05 for a high Reynolds number Rn ($Rn > 10^6$) and a large Keulegan-Carpenter number Kc with high roughness on a circular cylinder [33]. The Rn number and Kc number for the tested cases are summarized in Table 7.

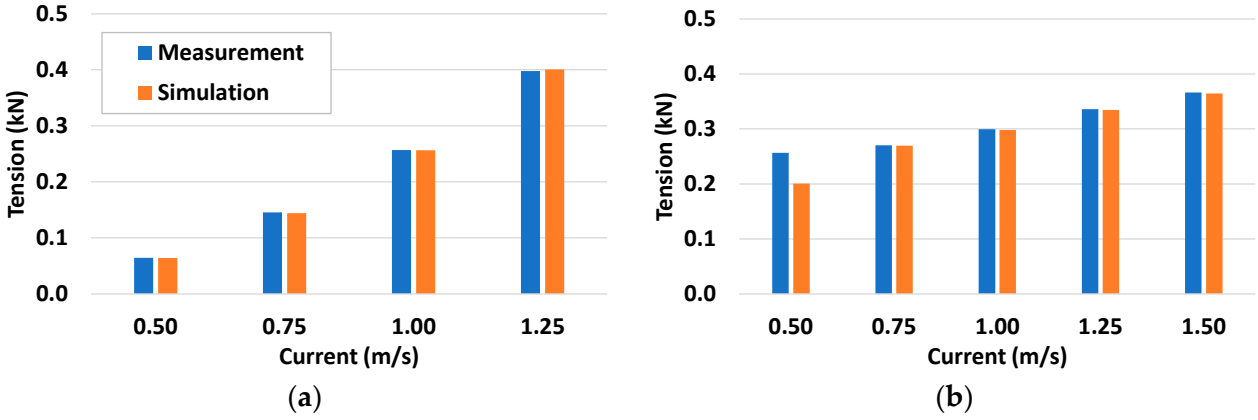

Figure 6. Comparison of tensions of full-scale oyster bag with marine growth in currents: (**a**) fixed oyster bag; (**b**) free-hanging oyster bag.

Table 7. Normal drag coefficients of oyster bag due to current and regular wave.

Parameter	LSWL	MSL	HSWL
Height, H (m)	6.04	8.31	10.93
Period, T (s)	11.16	11.16	11.16
Vw	3.24	3.80	4.37
Vc	0.98	0.98	0.98
Rn	1.32×10^6	1.50×10^6	1.68×10^6
Kc	118	133	149
Kc/C_{DS}	118	133	149
Ψ	1.00	1.00	1.00
Cd	1.00	1.00	1.00

4.3. Normal Drag Coefficients under Wave and Current

The method described in this Section follows the methods recommended in DNV [33]. The variations of drag under waves as a function of Kc number for a marine growth covered circular cylinder can be approximated by:

$$C_D = C_{DS}(\varepsilon) \cdot \Psi(K_c) \tag{3}$$

where Keulegan-Carpenter number is $K_c = \pi H/D$, H is the wave height, and D is the characteristic diameter. $C_{DS}(\epsilon)$ is the drag coefficient dependent on roughness of ϵ and the wake amplification factor $\Psi(K_c)$. Figure 7 indicates the variation of the wake factor as the function of Kc/C_{DS} for a circular cylinder [33]. The wake amplification factor can be applied to non-circular cylinders.

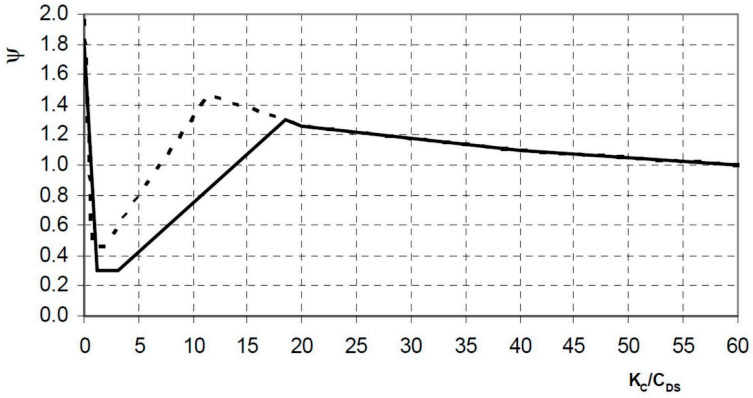

Figure 7. Wake amplification factor Ψ vs. Keulegan-Carpenter number *Kc* for smooth (C_{DS} = 0.65, solid line) and rough (C_{DS} = 1.05, dotted line) [33].

The drag coefficient for steady current, C_{DS}, is equal to the asymptotic value for infinitely large *Kc*. For the combined wave and in-line current, the increase in *Kc* due to the current may be considered as:

$$K_c = (V_w + V_c) \cdot T / D \quad (4)$$

where V_w is maximum wave velocity, V_c is current velocity, and T is wave period.

Knowing the drag coefficient C_{DS} of 1.0 under the current, the normal drag coefficient *Cd* on the oyster bag for the combined actions can be approximated. The results are summarized in Table 7. Here, wave particle velocity (V_w) is a velocity at z = −2.1 m, roughly a half of the oyster bag location from the water line. Based on the result, a current wave combined drag coefficient, *Cd*, is estimated to be 1.0.

4.4. Axial Drag Coefficient under Wave and Current

A total of eight regular waves, ranging from wave height 0.2 m to 0.5 m and from period 2 to 4.5 s, were generated for the wave basin tests with no currents, where the free-hanging full-scale bag was again used. Due to the limitation of high wave generation in the wave basin for the full-scale bag test, the small waves stated above were considered. Oyster bag line tensions were measured, and *Kc* numbers were calculated for the waves. Figure 8 compares the single oyster bag tensions between the measured and simulated ones under the wave conditions. Tension difference ranges are in 9~17% for Test No. 1 to 4 and 0.3~4% for Test No. 5 and Test No. 6. The *Kc* numbers from the tests are, however, smaller due to the small waves used than the *Kc* numbers in Table 7. Therefore, the measured *Kc* numbers were extrapolated for the higher *Kc* numbers.

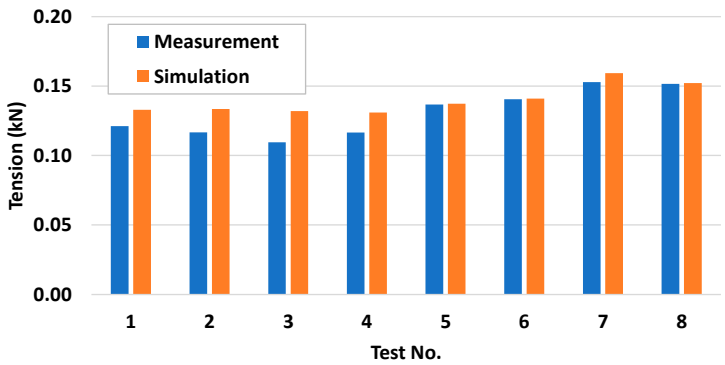

Figure 8. Measured and simulated tensions of the full-scale free-hanging oyster bag with marine growth in waves.

The next step was to derive the axial drag coefficient under the wave and current conditions in Table 7. For this purpose, a free-hanging single oyster bag with marine growth was modeled. The bag was attached at the middle of longline of 100 m long. Both ends of the longlines were fixed at 1.5 m below the water line. The bag's submerged location was determined from the wave basin test set-up. Here, the combined normal drag coefficient of 1.0 (Table 7) was set in the numerical model. Numerical simulations were repeated until the simulated tension under the wave and current converges to "total estimated tension", varying the axial drag coefficient but keeping the normal drag coefficient of 1.0. The "total estimated tension" was a linear sum of tension from the current and the wave separately, assuming that coupling effects between the waves and currents are small. The resulting axial *Cd* for LSWL, MSL, and HLWL were estimated to be 0.043, 0.034, and 0.027, respectively.

5. Numerical Modeling and Validation

OrcaFlex [29] software is used for modeling the farm component, including the lines, buoys, and oyster bags, and conducting the line-buoy-bag coupled time domain simulations. Hydrodynamic loads under a wave on the farm components are calculated by Morison's equation as:

$$F = \rho\, C_m\, \Delta\, \dot{u} + \frac{1}{2}\rho\, C_d\, A\, u\, |\dot{u}| \tag{5}$$

where the first term is inertia force, the second term is the drag force, F is the fluid force per unit length, ρ is the density of water, Δ is the mass of fluid displaced, $\dot{u}$ is the fluid acceleration, C_d is the drag coefficient, A is the drag area, and u is the fluid velocity. The fluid velocity can be decomposed to normal axial velocities. $C_m = 1 + C_a$ is the inertia coefficient and C_a is the added mass coefficient. The drag induced by the current with a velocity of U is calculated as:

$$F\,(t) = \frac{1}{2}\rho\, C_D\, U^2 A \tag{6}$$

In the farm model, all the farm lines and the oyster bags are modeled using the "line option" in OrcaFlex, imposing the properties in Table 4. Each line is made up of a number of segments with properties. The inertia and the added mass coefficients of the lines and oyster bags are 1.0, respectively. The drag coefficient of the lines are also set 1.7 considering the marine growth of the farm lines, whereas the drag coefficients of the oyster bags are used from the full-scale model test as described in the previous section. The buoys are modeled as 3-D buoys, allowing horizontal (surge and sway) and vertical (heave) motions. The added mass and drag coefficients of the buoys are 0.21 and 0.5, respectively.

The model is run for a sufficient time in a time domain under the waves and the currents defined in Table 3, and then the statistics of the responses are derived from the time histories, excluding the transient time. Additional modeling details of the complete model and the lumped model are described in the following sections.

5.1. Complete Model vs. Lumped Model

The total number of oyster bags and longline buoys of the whole farm of 200 m × 200 m size are 3781 (=199 × 19) and 1881 (=99 × 19), respectively. These arrangements cause significant modeling efforts, extremely long simulation times, and numerical instability in the time-domain simulations. For a practical approach, the following two methods have been implemented for the present analysis.

Complete model: All the buoys and oyster bags are modeled using the data in Tables 4–6. Thus, the total number of oyster bags and longline buoys per longline are the same as the numbers used for original marine farm and they will, thus, be 199 and 99 per line, respectively. The complete model is therefore used for the validation of the lumped model for a partial farm.

Lumped model: The lumped model is constructed by lumping (clustering) the oyster bags and longline buoys every 10m. Other components (main lines, anchor lines, cross

lines, and longlines) are not lumped, so they are the same as the original line configuration and properties. The physical properties of the longline buoys and the oyster bags lumped are equivalent to the complete model's values. In the lumped model, the lumped oyster bag length remains unchanged. Instead, the total volume and weight of the lumped bags are equivalent to the complete model values. The lumped model is used for the global analysis for the whole marine farm system. The main buoys and the side support buoys are modeled without lumping. Therefore, the original 80 buoys on the main lines are included in the lumped model of the whole farm. Figure 9 depicts an example of the complete and lumped model with two longlines, showing complete longline buoys and oyster bags and lumped buoys and bags.

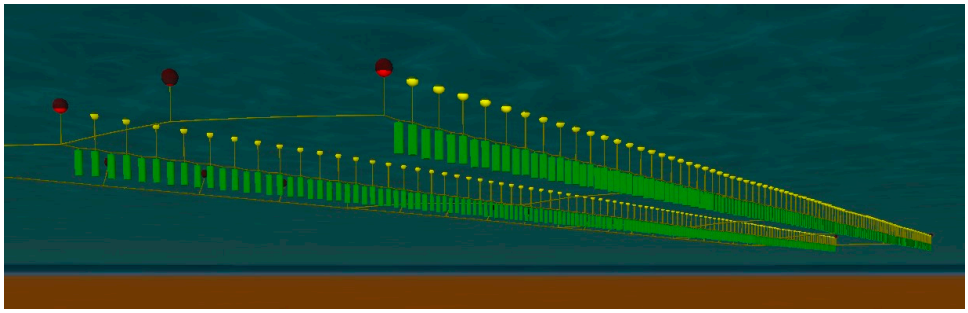

(**a**)

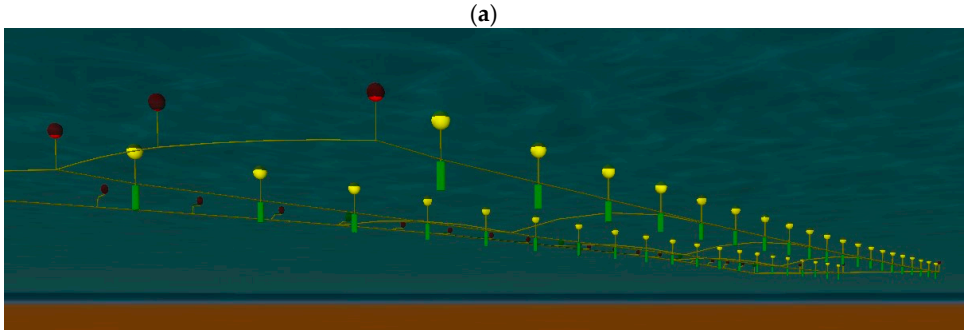

(**b**)

Figure 9. Farm model comparison: (**a**) complete model and (**b**) lumped model, showing the oyster bags (green), longline buoys (yellow) along with main lines and the side support buoys (red). For clarity, mooring lines are omitted.

5.2. Lumped Model Validation with Complete Model

A partial marine farm with two longlines was considered. The number of the mooring lines and cross lines were reduced for the validation simulation, and the mooring lines and cross lines are, thus, re-notated as shown in Figure 10. Figure 10 also shows the line displacements captured at a time instant of dynamic simulation for the MSL case in Table 7.

The normal coefficient of the oyster bag in the complete model is 1.0 in Table 7, while the axial drag coefficients are 0.043, 0.034, and 0.027 for LSWL, MSL, and HSWL. The wave and currents used are also provided in Table 7. The drag and inertia coefficients of each line are 1.7 and 1.0, respectively. The drag coefficients of the lumped bag in the lumped model were iteratively derived until the tensions from the lumped model converged with the values from the complete model.

The mooring anchor line tensions at N11 and the cross lines tensions at CL2 due to a regular wave and current are compared in Figure 11 for the wave dominant MSL and HSWL cases. The crossline tensions are at the north end of the line experiencing the highest loads due to the upstream location. It can be seen that the lumped model results of the anchor line and the crossline are in very good agreement with the complete model tensions.

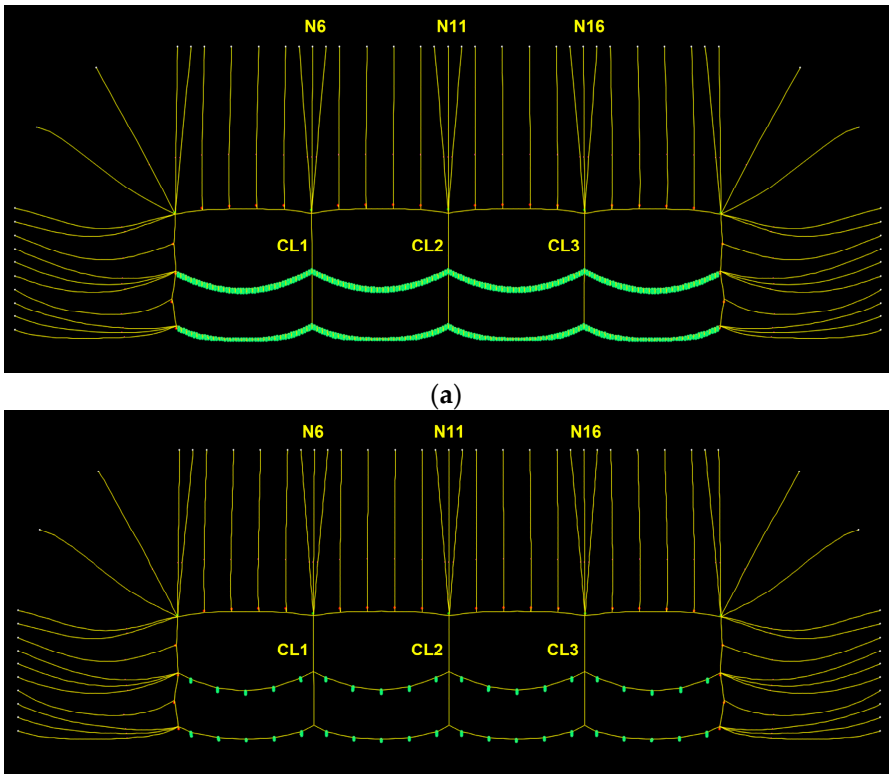

Figure 10. Partial farm example: (**a**) complete model and (**b**) lumped model, showing the farm line deformations at a time instant due to the wave and current from the farm north (270 deg).

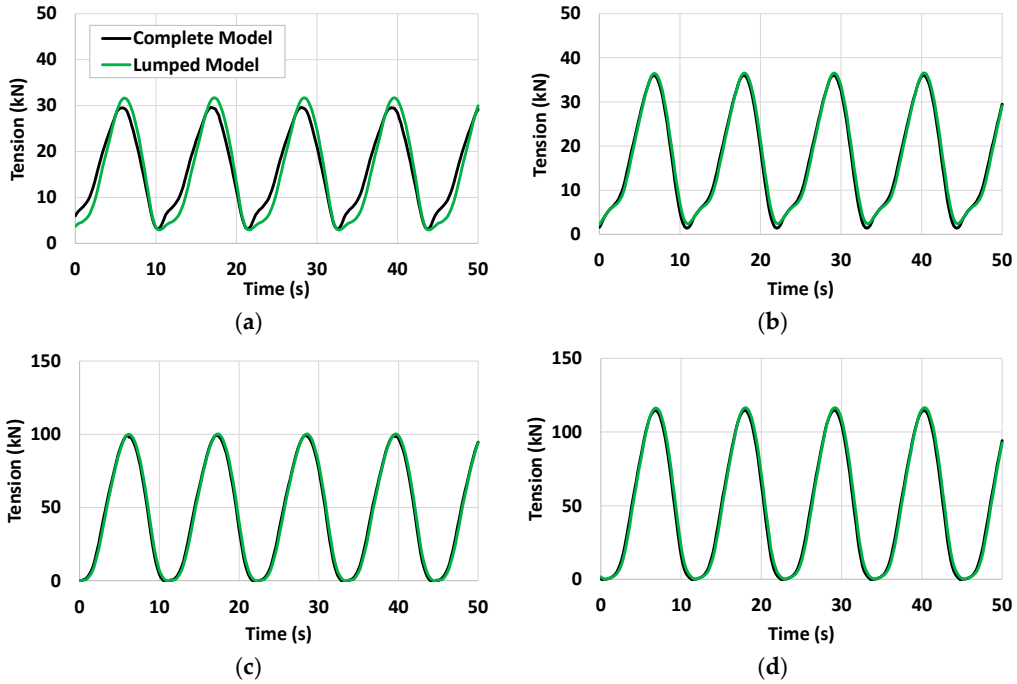

Figure 11. Tension time histories from the complete and lumped model simulations of the partial farm in regular wave: (**a**) anchor line N11 tension in MSL; (**b**) anchor line N11 tension in HSWL; (**c**) crossline CL2 tension in MSL; (**d**) crossline CL2 tension in HSWL. Regular wave and current are from the farm north (270 deg).

With the same drag coefficient setting, the irregular waves were tested with the complete and the lumped models. The tension time histories for the 10 min simulation are compared in Figure 12 for the anchor line N11 and the cross line CL2. The crossline tensions are at the 0 m from the north end of the line. The statistics of the tensions of the mean, standard deviation (STD) and peak are summarized in Table 8. It can be observed that the lumped model results once again agree well with the complete model values.

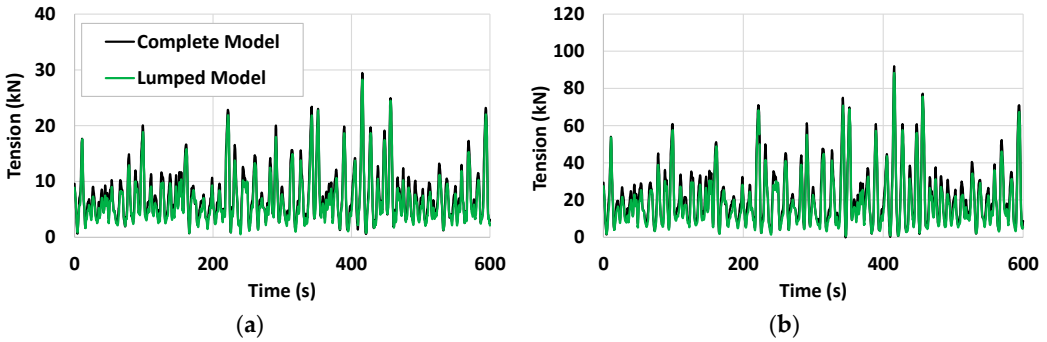

Figure 12. Time histories of tensions from the complete and lumped model simulations of the partial farm due to irregular waves in HSWL: (**a**) anchor line N11 tension; (**b**) crossline tension at the north end (0 m from the north). Irregular wave and current are from the farm north (270 deg).

Table 8. Mooring line and crossline tension statistics for a partial farm model (HSWL case, heading 270 deg).

Model	Location	Mean kN	STD kN	Peak kN
Complete	anchor line N11	7.57	4.68	29.46
Lumped	anchor line N11	6.70	4.40	28.28
Complete	crossline CL2 at 0 m	21.81	15.13	91.99
Lumped	crossline CL2 at 0 m	19.17	14.31	88.41

Based on the numerical model validations with the regular and irregular waves, it is confirmed that the lumped model approach developed in the present work can be extended to simulate the whole marine farm coupled analysis.

6. Results and Discussions

The whole pilot farm with 200 m × 200 m size is modeled using the lumped method described. Both oyster bags and longline buoys are lumped, as mentioned earlier. Therefore, total oyster bags and longline buoys in the model are 189 each. Other lines are modeled with no lumping so that main line, longline, crossline, and anchor lines modeled are 4, 9, 6, and 170, respectively. Length of the line segments for finite element analysis is set at 1.0 m.

A sample run was performed for the whole pilot farm with the lumped model approach for DLC-WM in Table 3 with a mis-alignment case (wave heading 315 deg and current heading 270 deg). This case may cause more complex couplings between the farm components compared to the co-directional case (270 deg), and it may be a good example to demonstrate the capability of the lumped model. Figure 13 presents the 2-dimensional and 3-dimensional deformations of the farm lines at a time instant of 20 s. Figure 13a also presents the slack anchor lines on the downstream side. In Figure 13b, the crest and the trough of the farm are clearly seen in the oblique waves flowing from the farm in the NW to SE direction.

Based on the sample run for feasibility, the present lumped model is repeated for the various load cases in Table 3, and its results and discussions are included in the following section.

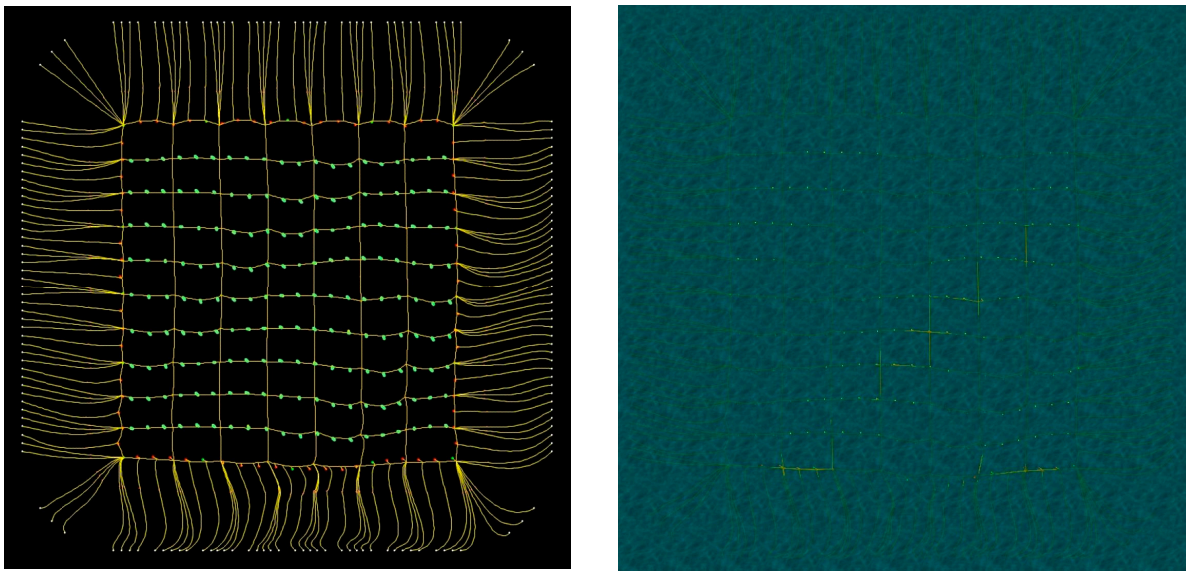

(a) (b)

Figure 13. Marine farm deformations simulated using the lumped model approach at a time instant 20 s: (**a**) 2-dimensional farm line deformations where the waves are removed for a clarity, which also presents the oyster bags (green) on the longlines, and main buoys (green) and side support buoys (red) on the main lines; (**b**) 3-dimensional shape deformations showing a part of the farm lines exposed to the wave surfaces along the oblique wave crest line.

6.1. Farm Line Strength

Each DLC of ULS in Table 3 was simulated in the time domain for the farm of 200 m × 200 m size with the lumped model. Duration of each simulation is 60 s, which may be sufficiently long to simulate the responses due to the regular waves considered. Simulations were conducted with the co-directional wave and current heading of 270 deg, flowing from the farm in the direction of north to south. Among the tensions of each farm line, the maximum tension on each line is selected, and its associated UF is calculated using Equation (1). The tensions and UF values of the farm lines are compared in Figure 14. It can be observed that the main line and the crossline experience larger loads among the lines. The anchor line exhibits the smallest tensions due to the load sharing by the high number of distributions of the anchor lines. This is our intended result (preferably a maximum tension of below 50 kN for the anchor line), enabling the utilization of a small size anchor readily available domestically. It is confirmed that the farm line UF values are below the requirement of 1.0, demonstrating the farm line strength design compliance. It is observed that the largest tension occurs in the DLC-WH (wave dominant and HSWL case). Therefore, the tensions of the DLC-WH case are selected and discussed in more detail in the analysis below.

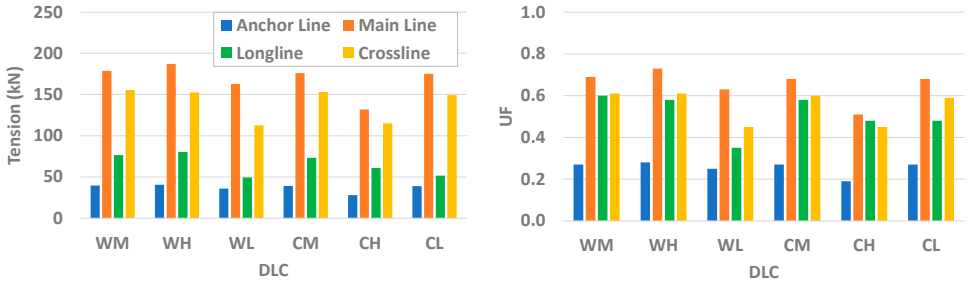

(a) (b)

Figure 14. Farm line tensions and UFs for the various DLCs in the ULS: (**a**) maximum tensions of each farm line; (**b**) associated UFs of the line.

Figure 15 compares the tensions of the anchor lines located on the farm's north and west sides. Anchor lines N1 and N22 are located at the west and east ends, while W1 and W21 are at the north and south ends. Others are located between the end points. It is seen that N1, N4, N7, N10, N13, N16, N19, and N22 have larger tensions compared to the neighboring lines. Those anchor line locations are at the connection points of the north end of the crossline so that the higher anchor line tensions at those points are mainly transferred from the crossline. The tensions on the west side vary but higher tensions are present, in general, on the downstream lines than the upstream lines. The result indicates that the anchor line tensions on the west (or east) side of the farm are affected by the longlines more in the downstream direction than the upstream. However, most loads from the longlines are transferred to the main lines, and the tension variations on the west (or east) side anchor lines are found to be small.

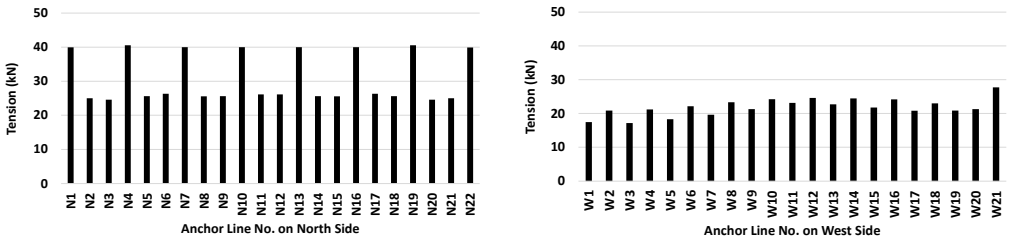

(**a**) (**b**)

Figure 15. Anchor tensions across the line for DLC-WH (ULS): (**a**) maximum tensions on north side anchor lines; (**b**) maximum tensions on west side anchor lines.

Among the four main lines, the tensions on three sides are compared in Figure 16, where, for example, a line notation of "N_0" is the north main line at 0 m from the west and "W_25" is the west main line at 25 m from the north end. The north and south lines show nearly an even distribution on the tensions across the line, while the tensions on the west lines decrease along the downstream direction. This may be due to the gradual accumulation of the loads toward the upstream locations, which are transferred from the downstream longlines.

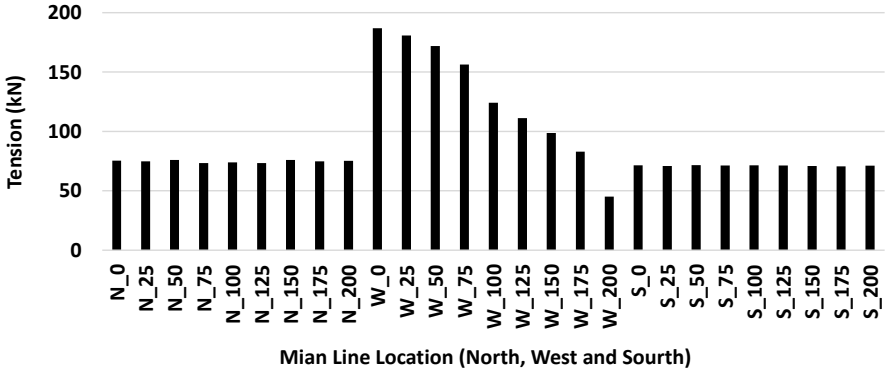

Figure 16. Main line maximum tensions across the line on north, west, and south sides for DLC-WH (ULS).

Four longlines of line 1, 3, 5, and 8 among a total of 9 lines are selected, and their tensions are compared in Figure 17. Longline 1 is the first line in the upstream, and others are in the downstream directions. Locations across each longline indicate the distance from the west end toward the east end. It is seen that longline 5 experiences the largest tension among the others. Longline 5 is located at the middle of the farm, which is about 80% of the incident wavelength. This indicates that the longlines with the oyster bags near the middle of the farm may have more coupled motions by the incident waves considered (Table 3). It

can also be observed that the tensions at both ends of the lines (0 m and 200 m) are greater than other locations across each line. This is due to a partial load transfer from the inside to outward locations of the longlines.

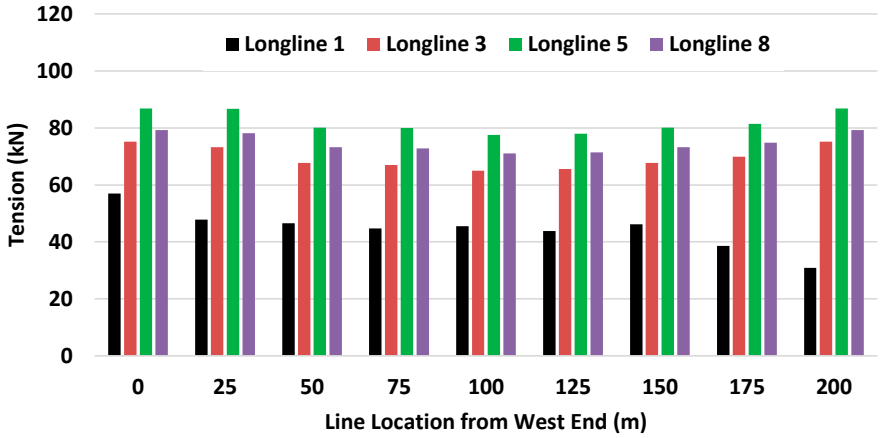

Figure 17. Longline tensions across the line for DLC-WH (ULS).

Figure 18 compares the crossline tensions of line 1 to 4. Here, the locations on each line are distances from the north end. The tensions on each line gradually decrease down the line to the south. Similar results are observed in the main line tensions on the west side (Figure 16). The crosslines of lines 3 and 4 in the middle of the farm width present higher tensions than other lines.

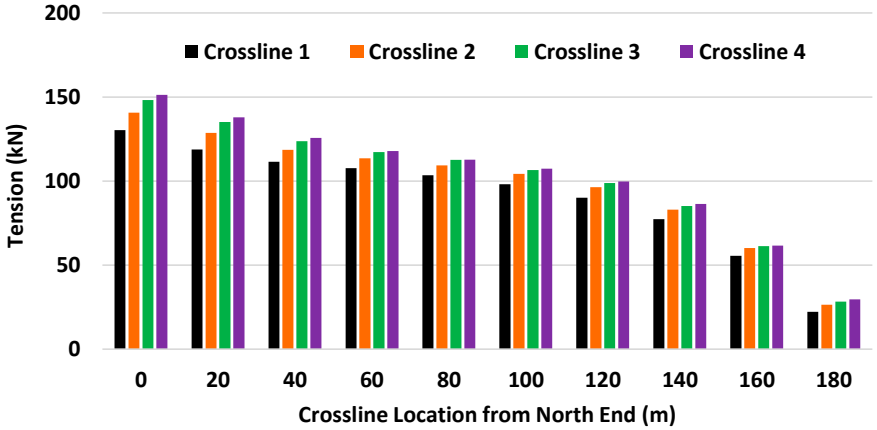

Figure 18. Cross line maximum tensions across the line for DLC-WH (ULS).

6.2. Marine Farm Line Fatigue

The fatigue lives of the farm lines are calculated with the line tensions and tension cycles using the TN curve in DNV [32], as presented in Equation (7):

$$NR^M = K \tag{7}$$

where N is number of cycles, and R is the ratio of the tension range to minimum breaking strength. Figure 19 presents the fatigue design T-N curve of a fiber rope, where the slope M and intercept K values are 13.46 and 0.259, respectively.

The site original scattered diagram is condensed to a total of 27 regular wave fatigue bins, as depicted in Figure 20. For the farm line fatigue analysis for FLS, misaligned waves (345 deg) and currents (270 deg) are considered. The misalignment headings chosen are based on the rose plots of the waves and currents of the site.

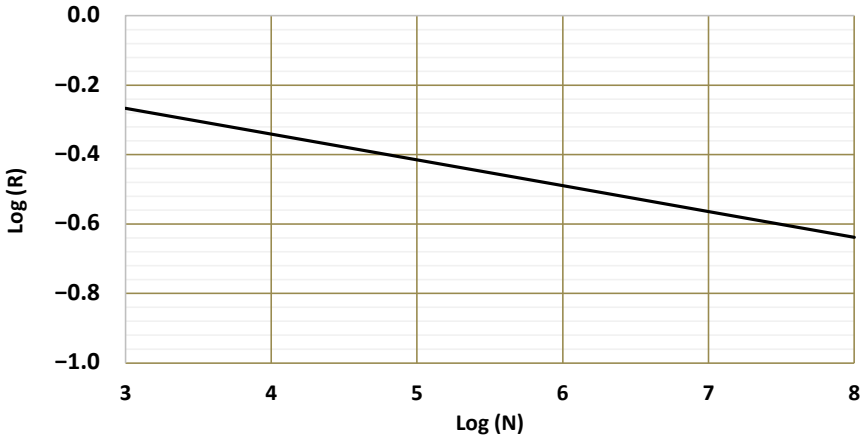

Figure 19. Farm line fatigue design T-N curve.

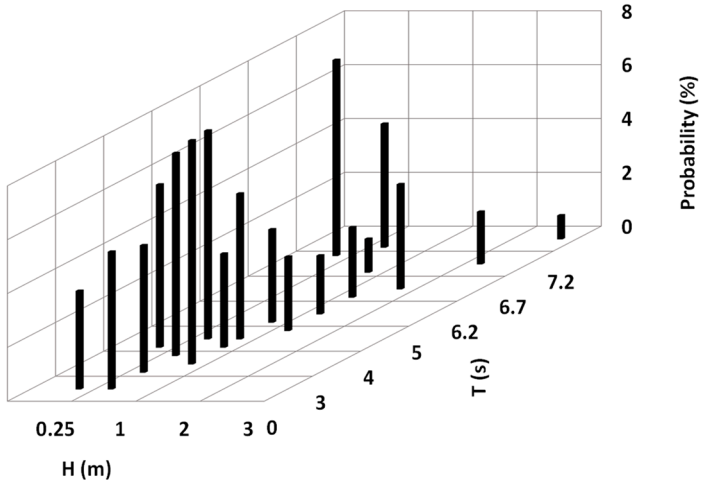

Figure 20. Scatter diagram of the site for fatigue analysis (FLS).

Figure 21 compares the lowest fatigue lives of the anchor lines, main lines, longlines, and cross lines. It is demonstrated that all the lines have very long fatigue lives that exceed the allowable minimum of 60 years. Among the lines, the longlines show the lowest lives so that the longlines are chosen to access the details of the life distribution (or damage distribution over the life). Fatigue lives along the longline from the west end to the east end points for the line 1, 5, and 9 are compared in Figure 22. The inner locations of the longlines present lower lives (or higher damages) than near the end locations, which may be due to higher dynamic coupling loads between components.

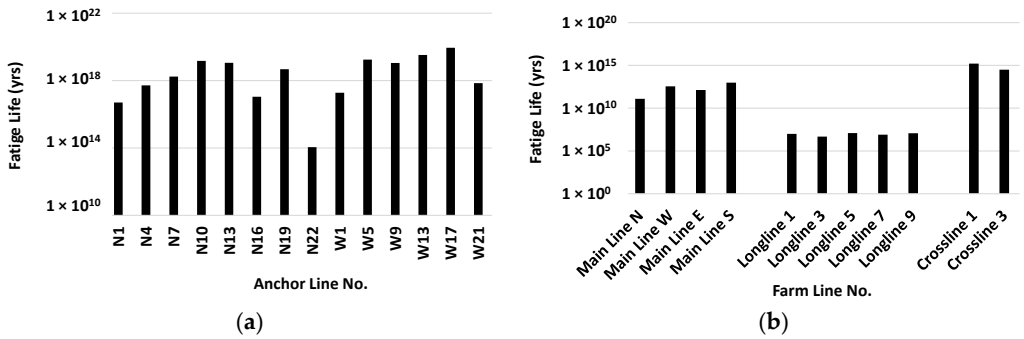

Figure 21. Minimum fatigue life of farm lines: (**a**) north and west anchor lines (**b**) main lines, longlines, and crosslines.

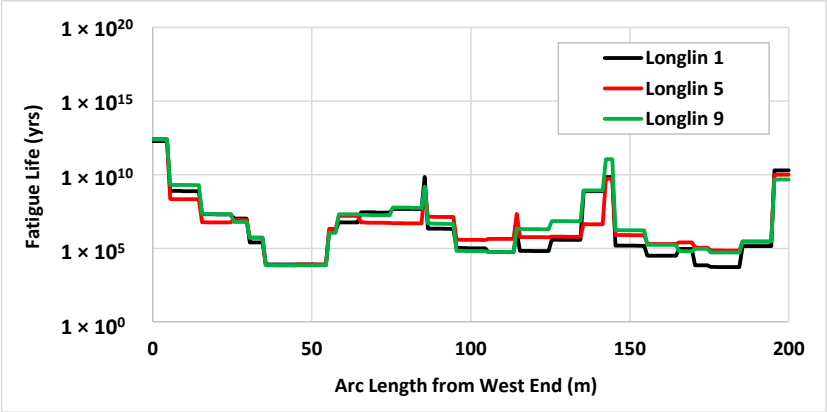

Figure 22. Fatigue life distribution of longlines along the arc length from the west end to the east end points.

6.3. Buoy Tension and Dispacement

There are a total of 80 buoys (main and side support buoys) installed along the farm boundary of the north, west, east, and south sides. The tensions of those buoy lines connecting the buoys and the main lines are compared in Figure 23a. Tensions are in the range of about 3.5 to 7.6 kN, which is smaller than the MBLs in Table 4. Among the scattered tension points, the upper points on the same side (e.g., N. side) indicate the tensions from the main buoys, while the lower points are from the side support buoys. This may be due to the larger size of the main buoy than the side support buoy. Four main buoys located at the middle of each side of the farm are selected and their horizontal motion trajectories from the mean position are plotted in Figure 23b. The main buoys in the east and west sides move around the mean position with an almost symmetrical pattern with each other. However, the main buoy in the south side experiences much higher motion compared to the upstream buoy (north side), which may be associated with higher displacements of the downstream longlines and main lines that are under less tension compared to the upstream lines.

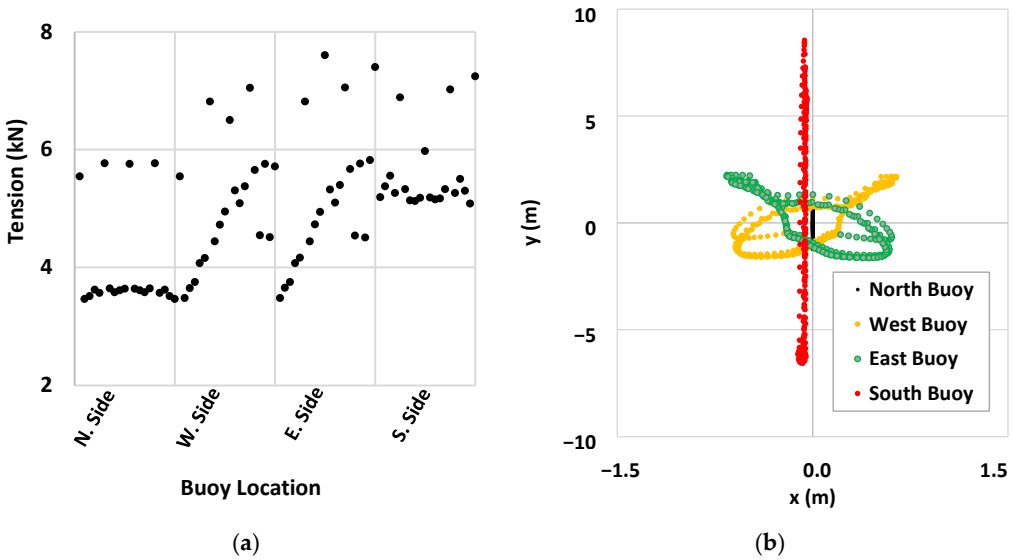

(**a**) (**b**)

Figure 23. Main buoy and side support buoy responses for DLC-WH (ULS): (**a**) main and side support buoy line tensions at various buoy locations; (**b**) motion trajectories of main buoys located at middle of the north, west, east, and south sides.

6.4. Farm Line Displacement

Displacement trajectories of the main lines and longlines (1, 5 and 9) are plotted in Figure 24 for DLC-WH. The locations selected are at the middle of the line or 100 m from the farm west. The motions are calculated from their original position before the environment is applied. There is a gradual increase in the motions from the upstream lines to the downstream lines. The north main line shows very small variation of the motion by the action of the anchor lines when compared to other lines, while significant motions on the south main line are observed in the environment direction (270 deg or *y*-axis). This result is associated with the line loading status. The north main line is under a taut condition by the anchor line action and the tensions transferred from the downstream lines, which allows a small displacement. However, a gradual slack from longline 1 to 9 is added to the south main line and causes the increase in the displacement on the south main line. The higher longline motions in the downstream side may result in damage to the culturing oyster bags during a storm.

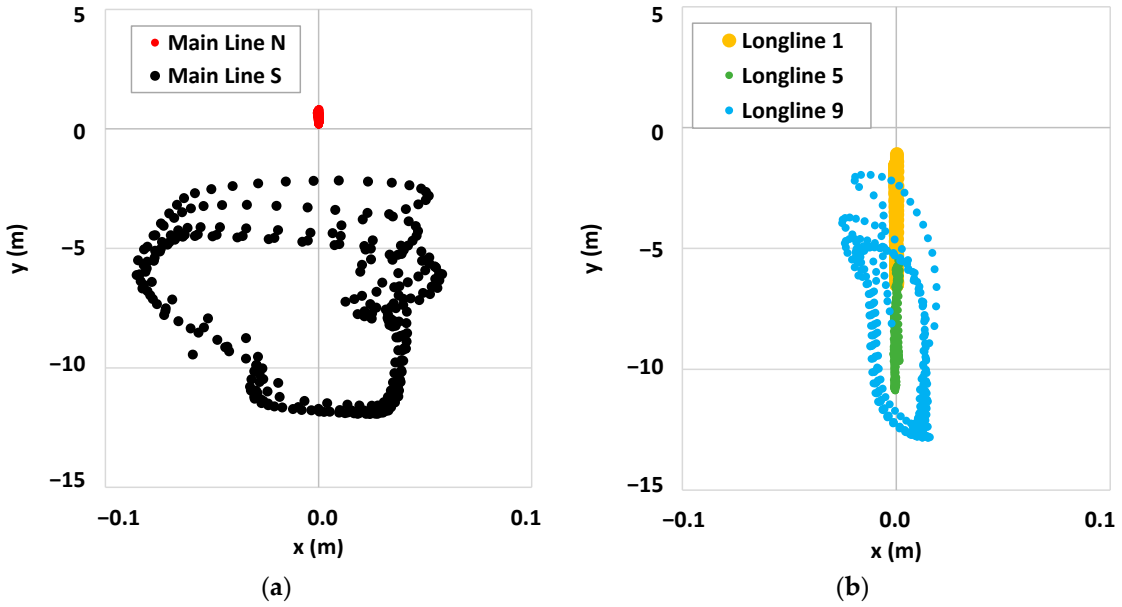

Figure 24. Main line and longline displacement trajectories at the middle of each line length for DLC-WH (ULS): (**a**) main line north and south; (**b**) longline 1, 5, and 9.

6.5. Wave-Current Coupled Efffect

The farm system load may be decomposed into loads induced by the wave and current. For this, simulations are repeated with current-only and wave-only cases. The results are compared in Table 9. Here, "current + wave" indicates a linear superimposed value of wave and current results, while "Current wave combined" are the results from the wave-current coupled analysis by combining them together, as described in this section. Four of the farm components of anchor line N10, crossline 3, main line west, and longline 5 are selected. The location details are specified Table 9. It can be seen that the wave loads are dominant over the current loads, which suggests that the longline farm design for an offshore installation primarily considers the effects of the wave. The linear superimposed values can be observed to be smaller than the results from the wave-current combined (coupled) case. The difference may be due to nonlinear coupling between the farm components, the wave, and the current under the extreme seas. It can be suggested that the analysis of the offshore longline farm considers both the wave and current together.

Table 9. Wave and current effect on the farm line tensions, heading 270 deg, DLC-WH (ULS).

Line Name	Location	Current	Wave	Wave + Current	Current Wave Combined	Difference
		kN	kN	kN	kN	%
Anchor line	N10	5.67	20.23	25.90	39.99	35.23
Crossline 3	0 m from north	28.48	89.03	117.51	167.97	30.04
Main line west	100 m from north	18.71	84.13	102.83	124.11	17.14
Longline 5	100 m from west	11.66	60.27	71.93	77.49	7.18

7. Conclusions

An offshore marine aquaculture farm with sub-surface longlines was designed to be installed in a fixed offshore wind farm in Korea in order to demonstrate the co-existence of a wind farm and a marine culture farm. The marine farm will cultivate multiple species of shellfish or macro-algae, but the present analysis considers an oyster farm. The oyster bags constructed with multiple compartments were attached to the longlines vertically. The farm with a cultivating area of 200 m $\times$ 200 m was considered as a pilot test farm. The farm was supported by multiple polypropylene ropes and buoys and moored with catenary mooring arrangements. Drag coefficients of the oyster bag were estimated through a wave basin test with a full-scale oyster bag and were used for input to the numerical model. A lumped model was developed to simulate the coupled effects between the farm components due to extreme waves and currents. The whole farm modeled with the lumped model approach was then simulated in design waves and currents of 50-year extreme seas and fatigue seas. It can be concluded that:

- The design wave approach can be used for the longline farm analysis, as its results are comparable to the values from the use of the irregular waves.
- The wave-current combined drag coefficients of the oyster bag may be determined by combining the laboratory test data under the wave and current individually, implementing the method in DNV [33].
- The axial (tangential) drag coefficient of the oyster bag decreases quickly with current speed. The axial drag, however, contributes to the considerable load increase of the farm lines under the wave and current environment, so that the axial coefficient is recommended to be included in the numerical analysis.
- Lumping the culturing units and buoys offers a practical approach to model the large and complex farm in terms of the modeling effort and the numerical stability in the time domain.
- With the analysis of a partial farm, the lumped model is validated with the complete model, indicating that the model can be applicable to estimate the loads on a longline farm.
- The lumped approach can provide an efficient tool to estimate the loads and motions of the longline farm components and can be used for a full-scale farm design.
- High water levels tend to cause higher tensions on the farm lines, but high tensions are also observed in lowest water level, which may be due to a large motion of the farm lines under relative slack compared to the taught condition.
- Line tensions of the wave current coupled are greater than the value from the liner superposition of tensions by wave only and current only. Therefore, large farm analysis will require the wave-current coupled model.
- Lines in the upstream are heavily loaded as the loads gradually accumulate from downstream. It is recommended that the material and size of the upstream lines are carefully selected in order to prevent line damage during a storm.
- Lines and buoys in the downstream experience high motions associated with a slack.
- The fatigue life of the polypropylene lines is extremely long, demonstrating a sufficient fatigue capacity of the farm lines used.
- Farm line strength and fatigue life meet the design requirements by the industry standards.

Author Contributions: Conceptualization, S.Y.B., S.A.S. and S.-H.S.; Formal analysis, S.Y.B.; Funding acquisition, S.-H.S.; Investigation, S.Y.B., J.P. and Y.-J.H.; Methodology, S.Y.B., S.A.S., S.-H.S., J.P. and Y.-J.H.; Project administration, S.-H.S., J.P. and Y.-J.H.; Supervision, S.Y.B., S.A.S. and S.-H.S.; Validation, S.Y.B. and S.A.S.; Writing—original draft, S.Y.B.; Writing—review and editing, S.A.S., S.-H.S. and J.P. All authors have read and agreed to the published version of the manuscript.

Funding: This study was partly supported by "Demonstration Project of Colocation of Offshore Wind Farm and Fisheries" by the Korea Institute of Energy Technology Evaluation and Planning (KETEP) and the Ministry of Trade, Industry & Energy (MOTIE) of the Republic of Korea (No. 20203040020130, PNS4260).

Institutional Review Board Statement: Not applicable.

Informed Consent Statement: Not applicable.

Data Availability Statement: Not applicable.

Acknowledgments: The first author gratefully thanks Seung-Ho Shin from KRISO for providing the model test results as well as guidance in various aspects of the marine farm configuration, farm line design, and coordination with the project teams.

Conflicts of Interest: The authors declare no conflict of interest.

References

1. Billing, S.-L.; Charalambides, G.; Tett, P.; Giordano, M.; Ruzzo, C.; Arena, F.; Santoro, A.; Lagasco, F.; Brizzi, G.; Collu, M. Combining wind power and farmed fish: Coastal community perceptions of multi-use offshore renewable energy installations in Europe. *Energy Res. Soc. Sci.* **2022**, *85*, 102421. [CrossRef]
2. Michler-Cieluch, T.; Krause, G.; Buck, B.H. Marine Aquaculture within Offshore Wind Farms: Social Aspects of Multiple-Use Planning. *GAIA-Ecol. Perspect. Sci. Soc.* **2009**, *18*, 158–162. [CrossRef]
3. Buck, B.H.; Troell, M.F.; Krause, G.; Angel, D.L.; Grotel, B.; Chopin, T. State of the Art and Challenges for Offshore Integrated Multi-Trophic Aquaculture (IMTA). *Front. Mar. Sci.* **2018**, *5*, 165. [CrossRef]
4. Buck, B.H.; Langan, R. *Aquaculture Perspective of Multi-Use Sites in the Open Ocean*; Springer: Cham, Switzerland, 2017; ISBN 978-3-319-51157-3. [CrossRef]
5. Buck, B.H.; Krause, G. Integration of Aquaculture and Renewable Energy Systems. In *Encyclopedia of Sustainability Science and Technology*; Springer: Berlin/Heidelberg, Germany; Cham, Switzerland, 2012; pp. 511–533. [CrossRef]
6. Buck, B.H.; Berg-Pollack, A.; Assheuer, J.; Zielinski, O.; Kassen, D. Technical realization of extensive aquaculture constructions in offshore wind farms: Consideration of the mechanical loads. In Proceedings of the OMAE06: 25th International Conference on Offshore Mechanics and Arctic Engineering, Hamburg, Germany, 4–9 June 2006.
7. Zheng, X.Y.; Lei, Y. Stochastic Response Analysis for a Floating Offshore Wind Turbine Integrated with a Steel Fish Farming Cage. *Appl. Sci.* **2018**, *8*, 1229. [CrossRef]
8. Zhai, Y.; Zhao, H.; Li, X.; Shi, W. Design and Dynamic Analysis of a Novel Large-Scale Barge-Type Floating Offshore Wind Turbine with Aquaculture Cage. *J. Mar. Sci. Eng.* **2022**, *10*, 1926. [CrossRef]
9. Stevens, C.; Plewb, D.; Hartstein, N.; Fredriksson, D. The physics of open-water shellfish aquaculture. *Aquac. Eng.* **2008**, *38*, 145–160. [CrossRef]
10. Raman-Nair, W.; Colbourne, B.; Gagnon, M.; Bergeron, P. Numerical model of a mussel longline system: Coupled dynamics. *Ocean Eng.* **2008**, *35*, 1372–1380. [CrossRef]
11. Zhu, L.; Huguenard, K.; Fredriksson, D.W. Dynamic Analysis of Longline Aquaculture Systems with a Coupled 3D Numerical Model. In Proceedings of the 29th International Ocean and Polar Engineering Conference, Honolulu, HI, USA, June 16, 2019.
12. Pribadi, A.B.K.; Donatini, L.; Lataire, E. Numerical Modelling of a Mussel Line System by means of Lumped-Mass Approach. *J. Mar. Sci. Eng.* **2019**, *7*, 309. [CrossRef]
13. Lien, E.; Fredheim, A. Development of Longtube Mussel systems for cultivation of mussels. In Proceedings of the OOA IV, Open Ocean Aquaculture IV Symposium, St. Andrews, NB, Canada, 17–20 June 2001.
14. Knysha, A.; Tsukrova, I.; Chambersa, M.; Swift, M.R.; Sullivana, C.; Drach, A. Numerical modeling of submerged mussel longlines with protective sleeves. *Aquac. Eng.* **2020**, *88*, 102027. [CrossRef]
15. Sulaiman, O.O.; Magee, A.; Bahrain, Z.; Kader, A.S.A.; Maimun, A.; Pauzi, A.G.; Wan Nick, W.B.; Othman, K. Mooring analysis for very large offshore aquaculture ocean plantation floating structure. *Ocean Coast. Manag.* **2013**, *80*, 80–88. [CrossRef]
16. Fredriksson, D.W.; Steppe, C.N.; Wallendorf, L.; Sweeney, S.; Kriebel, K. Biological and hydrodynamic design considerations for vertically oriented oyster grow out structures. *Aquac. Eng.* **2010**, *42*, 57–69. [CrossRef]
17. Gieschen, R.; Schwartpaul, C.; Landmann, J.; Fröhling, L.; Hildebrandt, A.; Goseberg, N. Large-scale laboratory experiments on mussel dropper lines in ocean surface waves. *J. Mar. Sci. Eng.* **2021**, *9*, 29. [CrossRef]
18. Landmann, J.; Ongsiek, T.; Goseberg, N.; Heasman, K.; Buck, B.B.; Paffenholz, J.-A.; Hildebrandt, A. Physical Modelling of Blue Mussel Dropper Lines for the Development of Surrogates and Hydrodynamic Coefficients. *J. Mar. Sci. Eng.* **2019**, *7*, 65. [CrossRef]

19. Cheng, W.; Xu, Y.; Mu, P. Experimental and numerical investigation of the dynamic responses of longline aquacultural structures under waves. *Ocean Eng.* **2023**, *276*, 114234. [CrossRef]
20. Sulaiman, O.O.; Magee, A.; Nik, W.B.W.; Saharuddin, A.H.; Kader, A.S.A. Design and Model Testing of Offshore Aquaculture Floating Structure for Seaweed Oceanic Plantation. *Biosci. Biotechnol. Res. Asia* **2012**, *9*, 477–494. [CrossRef]
21. Buck, B.H. Experimental trials on the feasibility of offshore seed production of the mussels Mytilus edulis in the German Bight: Installation, technical requirements and environmental conditions. *Helgol. Mar. Res.* **2007**, *61*, 87–101. [CrossRef]
22. Gagnon, M.; Bergeron, P. Observations of the loading and motion of a submerged mussel longline at an open ocean site. *Aquac. Eng.* **2017**, *78*, 114–129. [CrossRef]
23. Xu, T.-J.; Zhao, Y.-P.; Dong, G.H.; Li, Y.-C.; Gui, F.-K. Analysis of hydrodynamic behaviors of multiple net cages in combined wave–current flow. *J. Fluids Struct.* **2013**, *39*, 222–236. [CrossRef]
24. Hu, K.; Fu, S.; Xu, Y.; Chen, Y. Hydrodynamic response of multiple fish cages under wave loads. In Proceedings of the ASME 2014 33rd International Conference on Ocean, Offshore and Arctic Engineering OMAE2014, San Francisco, CA, USA, 8–13 June 2014.
25. Liu, Z.; Wang, S.; Soares, G. Numerical Study on the Mooring Force in an Offshore Fish Cage Array. *J. Mar. Sci. Eng.* **2022**, *10*, 331. [CrossRef]
26. Fredriksson, D.W.; DeCewa, J.; Swift, M.R.; Tsukrov, I.; Chambers, M.D.; Celikkol, B. The design and analysis of a four-cage grid mooring for open ocean aquaculture. *Aquac. Eng.* **2004**, *32*, 77–94. [CrossRef]
27. Ma, M.; Zhang, H.; Jeng, D.-S.; Wang, C.M. A semi-analytical model for studying hydroelastic behaviour of a cylindrical net cage under wave action. *J. Mar. Sci. Eng.* **2021**, *9*, 1445. [CrossRef]
28. Kim, T.-H. Motion characteristics of a Korean designed submersible fish cage system in waves and currents using numerical analysis. *Int. J. Aquat. Sci.* **2011**, *2*, 48–67.
29. OrcaFlex—Dynamic Analysis Software for Offshore Marine Systems. Available online: https://www.orcina.com/orcaflex/ (accessed on 8 April 2023).
30. *NS9415.E:2009*; Marine Fish Farms—Requirements for Site Survey, Risk Analyses, Design, Dimensioning, Production, Installation and Operation. Norwegian Standard: Oslo, Norway, 2009.
31. *DNVGL-RU-OU-0503*; Offshore Fish Farming Units and Installations. Det Norske Veritas (DNV): Høvik, Norway, 2020.
32. *DNVGL-OS-E301*; Position Mooring. Det Norske Veritas (DNV): Høvik, Norway, 2020.
33. *DNVGL-RP-C205*; Environmental Conditions and Environmental Loads. Det Norske Veritas (DNV): Høvik, Norway, 2020.
34. American Bureau of Shipping (ABS). *ABS Guide for Building and Classing—Aquaculture Installation*; American Bureau of Shipping: Houston, TX, USA, 2020.
35. *ISO16488*; Marine Finfish Farms—Open Net Cage—Design and Operation. International Standard (ISO): Geneva, Switzerland, 2015.
36. KEPRI. *Test Bed for 2.5 GW Offshore Wind Farm at Yellow Sea Design Basis Final Report*; TR.70B9.P2016.0299; KEPRI: Daejeon, Republic of Korea, July 2016. (In Korean)
37. KRISO—Korea Research Institute of Ships & Ocean Engineering (KRISO). Available online: https://www.kriso.re.kr/menu.es?mid=a20203000000 (accessed on 8 April 2023).